processes

MDPI

Article

Process Design and Kinetic-Based Simulation of a Coupled Biomass Gasification and Chemical Looping Ammonia Generation System

Zhongyuan Liu [1,2,*], Qingbo Yu [2], Huaqing Xie [2], Lunbo Luo [1], Ziwen Chen [1], Guangming Yu [1] and Chen Wang [1]

[1] Science and Technology Research Institute, China Three Gorges Corporation, Beijing 101199, China
[2] School of Metallurgy, Northeastern University, Shenyang 110819, China
* Correspondence: liuzhongyuan1997@foxmail.com

Abstract

Conventional ammonia production via the Haber–Bosch process is energy-intensive and carbon-heavy. Emerging biomass-based approaches offer a sustainable alternative but often lack rigorous system-level analysis based on actual reaction kinetics. This study presents a novel integrated process coupling biomass pyrolysis/gasification with Chemical Looping Ammonia Generation (CLAG) and waste heat recovery. Unlike previous models relying on simplified assumptions, this simulation incorporates experimental kinetic data for both N-absorption and N-desorption stages to ensure high fidelity. The system's energy and mass flows were rigorously evaluated using Aspen Plus. Results indicate that the gasification stage is optimal at an O_2/biomass molar ratio of 0.2 and 750 °C. In the CLAG unit, a higher N-absorption temperature (1600 °C) and α-Al_2O_3/C ratio (3:3) significantly enhance ammonia yield. Under these optimal conditions, the system achieves a remarkably low energy consumption of 10.12 GJ/t-NH_3 and specific CO_2 emissions of 3.2 t/t-NH_3—a reduction of over 60% compared to traditional coal-based routes. The integration of waste heat recovery is identified as a critical factor in minimizing net energy input. This work validates the feasibility of the biomass-based CLAG process as a low-carbon, energy-efficient pathway for sustainable ammonia synthesis.

Keywords: chemical looping ammonia generation; biomass cascade utilization; thermo-chemical process; sustainability

1. Introduction

Ammonia (NH_3) is indispensable to modern society, serving not only as the foundation for global fertilizer production but also increasingly as a promising carbon-free energy vector [1–4]. Due to its high hydrogen density (17.6 wt%), ease of liquefaction, and clean combustion profile, ammonia is regarded as a key enabler for decarbonizing "hard-to-abate" sectors, particularly maritime shipping [5–8]. The International Energy Agency (IEA) projects that low-carbon fuels, including ammonia, must satisfy nearly half of the shipping industry's energy demand by 2050 to meet net-zero targets [9,10]. However, current global production is dominated by the Haber–Bosch process, which operates under harsh conditions (400–500 °C, 150–300 bar) and relies heavily on fossil fuels [11]. This conventional route is energy-intensive (28–166 GJ/t NH_3) and accounts for significant CO_2 emissions (1.9–16.7 t/t NH_3), especially in coal-dominated energy structures like China's [12–14]. Consequently, developing novel, low-carbon ammonia synthesis pathways that fundamentally reduce energy consumption and carbon footprints is an urgent priority.

Check for updates

Received: 12 January 2026
Revised: 2 February 2026
Accepted: 6 February 2026
Published: 8 February 2026

Copyright: © 2026 by the authors. Licensee MDPI, Basel, Switzerland. This article is an open access article distributed under the terms and conditions of the Creative Commons Attribution (CC BY) license.

To bypass the harsh conditions of the Haber-Bosch process, various novel ammonia synthesis pathways have been extensively explored. Electrocatalytic nitrogen reduction (eNRR) has attracted significant attention for its ambient operation, with recent advances in single-atom catalysts and interface engineering lowering activation barriers [15,16]. Similarly, photocatalytic synthesis mimics natural nitrogen fixation by utilizing solar energy directly over semiconductor catalysts [17,18]. Furthermore, non-thermal plasma synthesis offers high reactivity by activating the inert N≡N bond via energetic electron impact [19,20]. However, despite these advances, fundamental bottlenecks remain. Electrocatalysis is currently plagued by extremely low Faradaic efficiency and yield, primarily due to the vigorous competition from the Hydrogen Evolution Reaction (HER) in aqueous electrolytes [21]. Photocatalytic methods suffer from poor solar-to-chemical quantum efficiency and rapid carrier recombination [22]. Plasma-driven synthesis, while fast, is limited by high energy consumption and low overall energy efficiency [23].

Chemical Looping Ammonia Generation (CLAG) has emerged as a disruptive technology designed to circumvent the thermodynamic equilibrium limits and kinetic barriers of the Haber–Bosch process [24,25]. By decoupling ammonia synthesis into two distinct steps—nitrogen absorption (N-absorption) and nitrogen desorption (N-desorption)—CLAG allows for operation at atmospheric pressure and more flexible temperature ranges. Among the various configurations, the water-based CLAG (H_2O-CLAG) route utilizing solid carbon reductants offers superior economic potential compared to hydrogen-based routes, as it eliminates the need for expensive hydrogen production steps [26,27]. Recent experimental studies have highlighted biochar as an ideal reductant due to its porous structure and low SiO_2 content [28,29]. Furthermore, the introduction of carrier materials, such as α-Al_2O_3, has been shown to not only facilitate heat transfer but also catalytically promote N-desorption and inhibit ammonia decomposition, thereby enhancing the net yield [30,31].

Recognizing the potential of CLAG, several system-level studies have been conducted to evaluate its integration efficiency. Weng et al. designed a hybrid system coupling chemical looping air separation with CLAG, reporting an ammonia selectivity of nearly 80% [32]. Similarly, Fang et al. and Wen et al. developed integrated polygeneration systems, demonstrating the theoretical feasibility of coupling CLAG with urea synthesis or power generation to achieve high energy efficiencies [33,34].

However, a critical limitation persists in these system-level analyses. The majority of existing process simulations rely on idealized assumptions to predict reactor performance. In these simplified models, the conversion rates of N-absorption and N-desorption are often preset as fixed values or linear functions of temperature, neglecting the complex, non-linear reaction kinetics influenced by the carbon source's microstructure, reactant ratios, and carrier interactions. Such oversimplification compromises the fidelity of the simulation, potentially leading to inaccurate predictions of heat duties and mass balances in practical engineering scenarios.

To bridge the gap between experimental reaction characteristics and system-level process design, this study presents a rigorous simulation of a biomass-based CLAG system coupled with gasification and waste heat recovery. Unlike previous theoretical models, this work integrates experimentally derived reaction kinetics for both the N-absorption (biochar reactivity) and N-desorption steps (α-Al_2O_3 effects) into the Aspen Plus environment. This approach allows for a realistic quantification of energy and mass flows under varying operating conditions. The study systematically optimizes key parameters—including gasification temperature, O_2/biomass ratio, and the α-Al_2O_3/C circulation ratio—to minimize specific energy consumption and CO_2 emissions. By establishing a kinetically grounded process model, this work provides a robust theoretical basis and data support for the scale-up and industrialization of sustainable biomass-to-ammonia technologies.

2. Process Simulation and Model Development

2.1. System Description and Simulation Assumptions

The conceptual framework of the biochar-based CLAG system coupled with biomass gasification is illustrated in Figure 1. The integrated process is functionally divided into three primary subsystems: (i) Biomass Pretreatment and Pyrolysis/Gasification, (ii) Chemical Looping Ammonia Generation (CLAG), and (iii) Waste Heat Recovery.

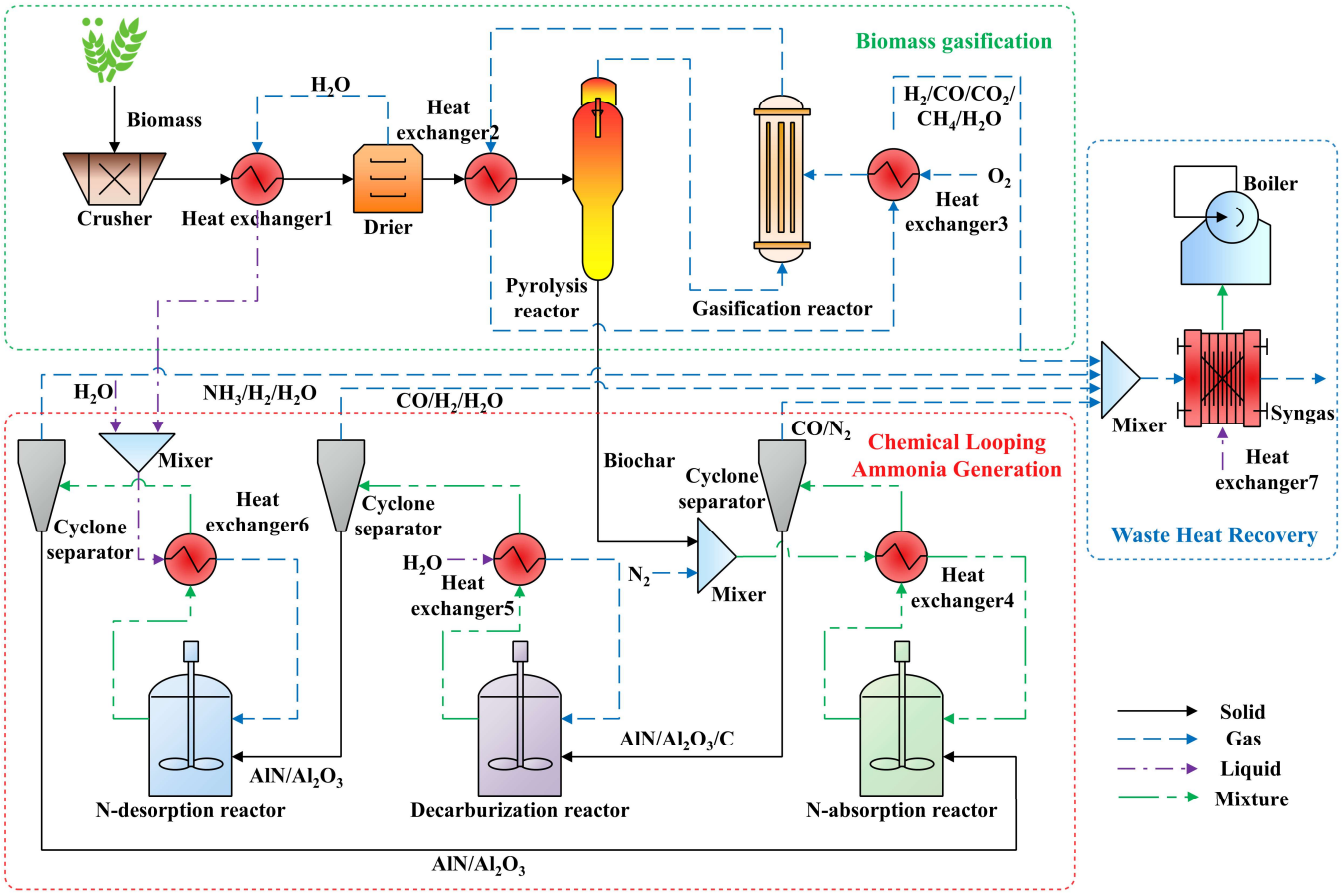


Figure 1. Schematic flow diagram of the system for biochar-CLAG.

In the initial stage, biomass is comminuted and dehydrated in a drying unit to meet moisture requirements. The dried feedstock undergoes pyrolysis in an inert nitrogen atmosphere, fractionating into biochar, bio-oil, and biogas. The high-quality biochar serves as the solid reductant for the subsequent CLAG unit, while the volatile components (bio-oil and biogas) are diverted to a gasification reactor. Here, they undergo partial oxidation with oxygen to produce syngas.

The core CLAG loop comprises the Nitrogen Absorption (N-absorption) and Nitrogen Desorption (N-desorption) reactors. In the N-absorption reactor, biochar, N_2, and the nitrogen carrier (α-Al_2O_3) react to form aluminum nitride (AlN) and CO. Following gas–solid separation via a cyclone, the solid stream (containing AlN, unreacted carbon, and carrier) proceeds to a decarburization reactor. This intermediate step utilizes steam to gasify residual carbon, preventing carbon contamination in the subsequent ammonia synthesis step. The purified solids then enter the N-desorption reactor, where AlN reacts with steam to regenerate α-Al_2O_3 and release NH_3. The regenerated carrier is recycled to the N-absorption reactor, initiating the subsequent cycle.

To maximize thermal efficiency, a rigorous heat integration strategy is employed. High-temperature product gas streams from reactors are utilized to preheat incoming cold streams.

Furthermore, a terminal waste heat recovery unit is installed to capture residual enthalpy from the product gas streams, thereby minimizing the net energy penalty of the system.

2.2. Model Assumptions and Simulation Constraints

To establish a robust steady-state simulation in Aspen Plus while maintaining computational feasibility, the following engineering assumptions and constraints were adopted:

1. The system operates under steady-state conditions. Pressure drops across reactors, cyclones, and piping are neglected in this conceptual design phase. This simplification is adopted because detailed geometric parameters (e.g., pipe layouts and lengths) are undefined at this stage. While it is acknowledged that practical operation requires auxiliary power for blowers, preliminary order-of-magnitude analysis indicates that this mechanical energy input is substantially lower than the system's dominant thermal energy duties (reaction enthalpy). Furthermore, this omission does not affect the fundamental comparative advantage of the CLAG process over the Haber-Bosch route, which requires massive energy for high-pressure gas compression (150–300 bar).
2. Chemical reactions are modeled based on their respective governing principles: thermodynamic equilibrium is assumed for biomass gasification, while conversion levels for the CLAG process are strictly defined by experimental kinetic data. Phase separations are assumed to be ideal.
3. Biomass is modeled as a non-conventional component based on its ultimate and proximate analyses. The O_2/Biomass molar ratio (O_2/B) in the gasification unit is normalized to the molar flow rate of carbon in the feedstock.
4. The product spectrum of biomass gasification is restricted to major thermodynamic species: O_2, CO, CO_2, CH_4, C_2H_6, C_3H_8, COS, SO_2, H_2S, NH_3, N_2, H_2O, and H_2 [35].
5. In the decarburization unit, complete conversion of residual carbon with steam is assumed, yielding CO and H_2.
6. The waste heat recovery unit is designed to cool process gas streams to a discharge temperature of 120 °C to prevent acid dew point corrosion while maximizing energy recovery.

2.3. Physical Property Parameters and Model Construction

The simulation involves a complex mixture of conventional fluids and non-conventional solids (biomass/char), requiring a tailored approach for physical property estimation. The MIXCINC stream class was selected to handle the heterogeneous streams. The Redlich-Kwong-Soave with Boston-Mathias alpha function (RKS-BM) equation of state was employed for property estimation of conventional components [36], while the DCOALIGT and HCOALGEN models were utilized for enthalpy and density calculations of non-conventional biomass components [35].

The comprehensive Aspen Plus flowsheet is presented in Figure 2. The simulation strategy for key units is detailed below:

Biomass Pretreatment: The wet biomass (WET-BIO, 18,000 kg/h) is processed through a simulated dryer (modeled via a Heater and Flash block). Given that the proximate analysis in Table 1 corresponds to dried biomass, the model incorporates an initial moisture content of approximately 30% to accurately represent the raw feedstock [29]. Consequently, the drying unit is configured to reduce the moisture level to the target specification at 105 °C. The evaporated water is recovered as a steam source for the CLAG section.

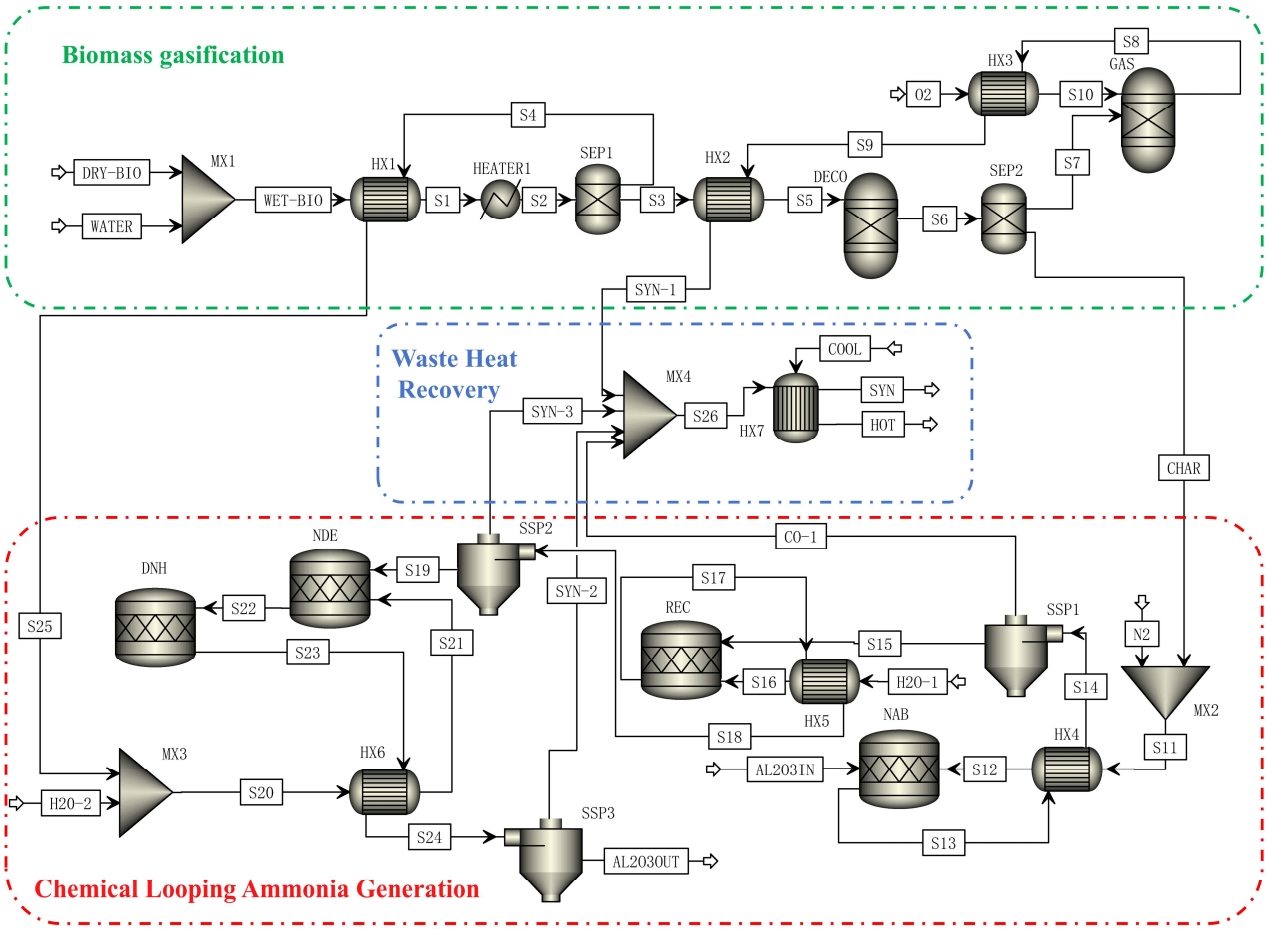


Figure 2. Process modeling in Aspen Plus software.

Table 1. Analysis of biomass.

Proximate Analysis	wt%	Ultimate Analysis (d.b.)	wt%
Fixed carbon (d.b.)	14.48	Carbon	48.50
Moisture (a.r.)	4.97	Hydrogen	7.94
Volatile matter (d.b.)	80.46	Oxygen (by difference)	41.50
Ash (d.b.)	0.09	Nitrogen	2.05
		Total sulfur	0.01

Pyrolysis and Gasification: The pyrolysis reactor is modeled using an RYield block (DECO), which decomposes the non-conventional biomass into constituent elements based on experimental pyrolysis yields obtained at 700 °C (heating rate 10 °C/min, holding time 30 min) [29]. The biochar yield is fixed at 21.4 wt% relative to the dry biomass. The gasification of gaseous intermediates (bio-oil and biogas) is simulated using an RGibbs reactor (GAS), which calculates the product distribution by minimizing Gibbs free energy.

The CLAG section integrates experimentally determined reaction characteristics: N-Absorption (NAB): Modeled using an RStoic block. The carbon conversion efficiency is not arbitrary but is rigorously defined as a function of temperature and α-Al_2O_3/C ratio, derived from our fixed-bed experimental correlations [29].

Decarburization (REC): An RStoic block simulates the removal of residual carbon.

N-Desorption and Ammonia Decomposition (NDE & DNH): This stage is critical for accurate yield prediction. It is modeled as two series RStoic blocks. The first (NDE) simulates the hydrolysis of AlN at 1075 °C for complete conversion. The second (DNH) accounts for

the thermal decomposition of NH_3. Crucially, the NH_3 decomposition extent is linked to the α-Al_2O_3 mass fraction based on our kinetic experimental data (Figure 3 and Table 2), capturing the catalytic effect of the nitrogen carrier material [31]. It is important to emphasize that the kinetic correlations employed in this simulation—including the biochar reactivity for N-absorption and the NH_3 decomposition rates in Table 2—were all derived from laboratory-scale fixed-bed experiments. These experiments utilized thin particle layers to eliminate external mass transfer and internal diffusion limitations, thereby capturing the intrinsic reaction kinetics of the nitrogen carrier system. While industrial applications typically favor fluidized-bed reactors to enhance heat and mass transfer, utilizing intrinsic kinetics in this simulation establishes a rigorous thermodynamic baseline. It represents the theoretical maximum conversion achievable when transport resistances are minimized, providing a reliable foundation for this system-level process evaluation.

This hybrid modeling approach—combining thermodynamic equilibrium for gas phase reactions with experimental kinetics for gas–solid looping reactions—ensures the simulation fidelity significantly exceeds that of purely theoretical models.

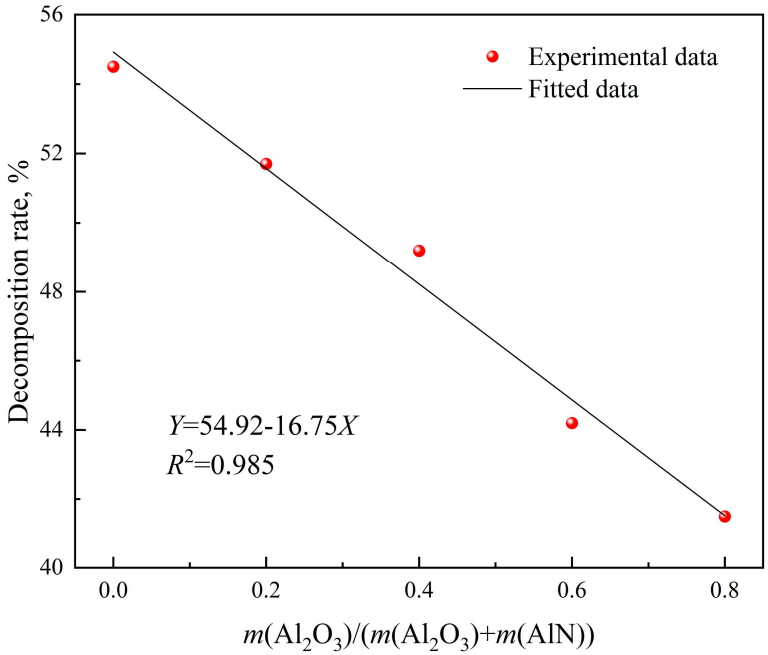


Figure 3. NH_3 decomposition rate versus α-Al_2O_3 loading at 1075 °C.

Table 2. Decomposition rates of NH_3 corresponding to different simulation conditions in the CLAG module.

Temperature, °C	α-Al_2O_3:C	C Conversion, %	Mass Fraction of α-Al_2O_3, %	NH_3 Decomposition Rate, %
1400	1:3	21.9	81.6	41.3
	1.5:3	30.4	83.1	41
	2:3	37.5	84.4	40.8
	2.5:3	47.1	84.3	40.8
	3:3	54.5	84.9	40.7
1450	1:3	29.6	74.8	42.4
	1.5:3	36.3	79.6	41.6
	2:3	47.4	80	41.5
	2.5:3	54.6	81.6	41.2
	3:3	61.6	82.8	41.1

Table 2. *Cont.*

Temperature, °C	α-Al_2O_3:C	C Conversion, %	Mass Fraction of α-Al_2O_3, %	NH_3 Decomposition Rate, %
1500	1:3	36.0	68.9	43.4
	1.5:3	46.5	73.5	42.6
	2:3	55.2	76.6	42.1
	2.5:3	60.1	79.7	41.6
	3:3	71.3	79.9	41.5
1550	1:3	45.7	59.6	44.9
	1.5:3	54.6	68.5	43.4
	2:3	60.7	74.1	42.5
	2.5:3	71.9	75.5	42.3
	3:3	81.0	77.1	42
1600	1:3	57.8	47.6	46.9
	1.5:3	67.6	60.3	44.8
	2:3	77.7	66.2	43.8
	2.5:3	88.0	69.6	43.3
	3:3	95.5	72.7	42.7

3. Results and Discussion

3.1. Performance Characteristics of Biomass Gasification

The biomass gasification unit serves as the energy and feedstock provider for the integrated system. Its performance—quantified by syngas composition and thermal balance—was rigorously evaluated against the gasification temperature and O_2/Biomass (O_2/B) molar ratio.

3.1.1. Syngas Yield and Compositional Analysis

Figure 4 illustrates the dependence of syngas yield and composition on operating parameters. As the O_2/B ratio increases, the total gas yield rises significantly (Figure 4a). This trend is attributed to the enhanced extent of partial oxidation reactions, which promote the fuller conversion of gaseous intermediates (bio-oil and biogas) into syngas components. Regarding the hydrocarbon species, the residual CH_4 content exhibits a decline with increasing temperature and oxygen supply. Mechanistically, this is attributed to the competition between formation and consumption reactions. Elevated temperatures thermodynamically promote the highly endothermic steam methane reforming reaction ($CH_4 + H_2O \rightarrow CO + 3H_2$), driving the equilibrium towards the deep decomposition of CH_4. Simultaneously, a higher O_2 concentration accelerates partial oxidation reactions, directly consuming methane to form syngas components.

The mole fraction of H_2 (Figure 4b) exhibits a declining trend with increasing O_2/B ratio, mechanistically explained by the oxidation of H_2 to H_2O at higher oxygen availability. Notably, compared to the O_2/B ratio, the effect of temperature on H_2 concentration is relatively marginal. This insensitivity arises from the counterbalancing effects of high-temperature reforming reactions (which promote H_2 generation) and the thermodynamic suppression of the exothermic Water-Gas Shift reaction (which limits H_2 yield). In contrast, the CO mole fraction (Figure 4c) is significantly favored by both higher temperatures and lower O_2/B ratios. The positive correlation with temperature is driven by the endothermic Boudouard reaction ($C + CO_2 \leftrightarrow 2CO$) and steam reforming reactions, which are thermodynamically promoted at elevated temperatures according to Le Chatelier's principle.

A critical metric for environmental performance is the CO_2/CO molar ratio (Figure 4d). High temperatures and low O_2/B ratios effectively suppress this ratio. This indicates that

under these conditions, the system favors the production of high-value CO fuel over inert CO_2, thereby enhancing the carbon utilization efficiency of the biomass feedstock.

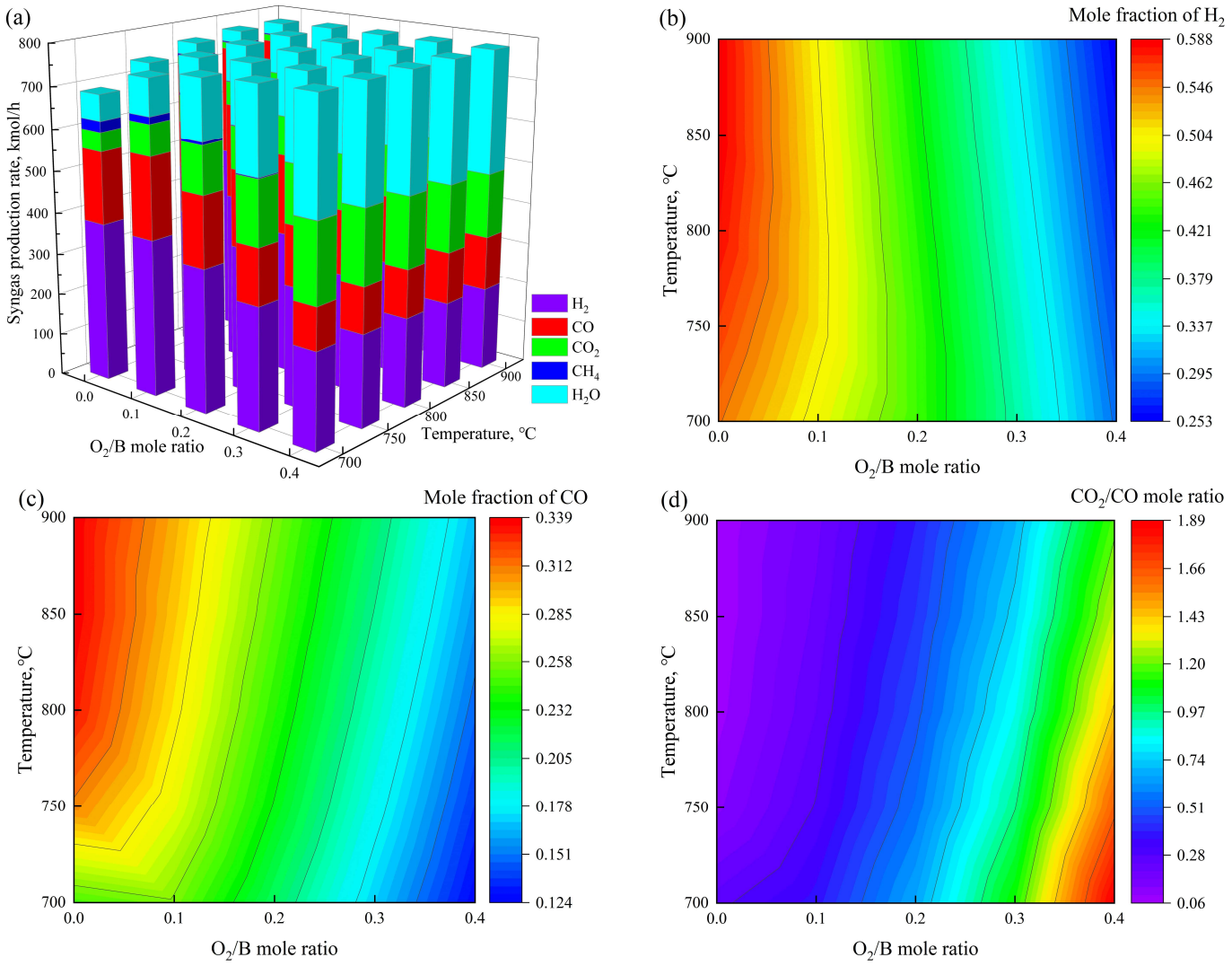


Figure 4. Effects of gasification temperature and O_2/B molar ratio on syngas characteristics. (**a**) Syngas composition and individual gas yields, (**b**) mole fraction of H_2, (**c**) mole fraction of CO, (**d**) CO_2/CO molar ratio.

3.1.2. Energy Balance and Optimal Operating Point

The trade-off between gas quality and energy efficiency is depicted in Figures 5 and 6. The Higher Heating Value (HHV) of the product gas decreases with increasing O_2/B ratio due to the dilution effect of combustion products (CO_2 and H_2O).

Figure 6 analyzes the heat duty of the gasification reactor (GAS). The negative values confirm the exothermic nature of the process. To achieve an autothermal operation for the combined pyrolysis-gasification stage, the heat released by the gasifier must compensate for the endothermic heat demand of the pyrolysis unit. This heat duty (calculated as 94.47 GJ/h) represents the fixed enthalpy difference ($\triangle H$) between the feedstock and the constant distribution of pyrolysis products at 700 °C [29]. The intersection analysis (dashed line in Figure 6) reveals that a gasification temperature of 750 °C coupled with an O_2/B molar ratio of 0.2 establishes the requisite thermal equilibrium. Under these specific conditions, the system effectively balances high syngas quality with energy self-sufficiency, thereby eliminating the reliance on external fuel combustion and defining the optimal thermodynamic state for process integration.

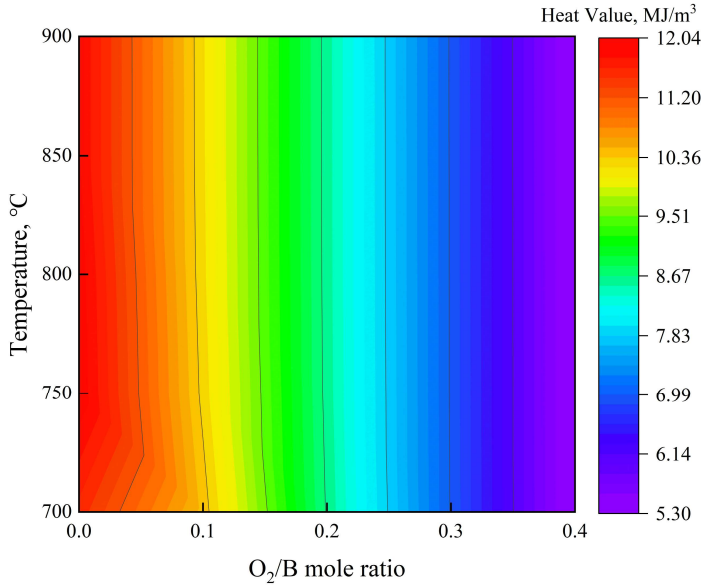


Figure 5. Effect of gasification temperature and O_2/B molar ratio on the higher heating value of the product gas.

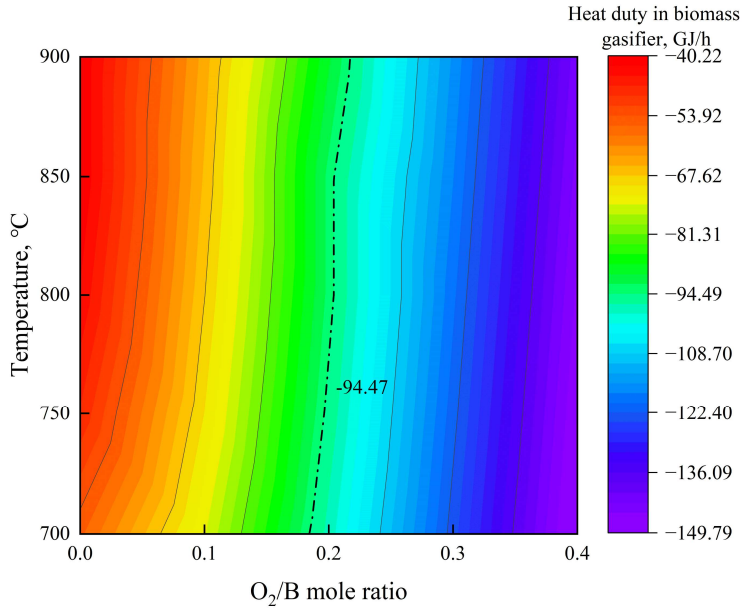


Figure 6. The effect of gasification temperature and O_2/B molar ratio on the heat duty of GAS.

3.2. Optimization of the Chemical Looping Ammonia Generation (CLAG) Process

The performance of the CLAG unit was evaluated based on the experimental kinetic data. While the CLAG process involves multiple reaction steps, the operating conditions for the decarburization and N-desorption stages were fixed based on specific process constraints and prior experimental optimizations. Specifically, the decarburization reactor was maintained at 750 °C solely to remove residual carbon without interfering with the primary nitrogen cycle. Similarly, the N-desorption temperature was set at 1075 °C, a value experimentally verified to maximize ammonia yield by balancing AlN hydrolysis kinetics against ammonia decomposition [31]. Consequently, the optimization study focused on the two remaining governing variables that primarily determine the system's overall efficiency and thermal balance: the N-absorption temperature and the solid circulation ratio (α-Al_2O_3/C).

3.2.1. Ammonia and Hydrogen Yield Analysis

Figure 7 reveals a competitive relationship between NH_3 and H_2 production. Increasing the N-absorption temperature and α-Al_2O_3/C ratio significantly enhances NH_3 yield. This enhancement is primarily driven by kinetic factors; higher temperatures overcome the activation energy barrier of the endothermic N-absorption reaction ($3C + Al_2O_3 + N_2 \rightarrow 2AlN + 3CO$), leading to higher carbon conversion and AlN formation. Simultaneously, a higher α-Al_2O_3/C ratio promotes AlN formation by increasing the concentration of gaseous oxygen intermediates derived from α-Al_2O_3 decomposition, which lowers the activation energy for carbon conversion [37]. Furthermore, the excess carrier material plays a crucial role in the subsequent stage by inhibiting the thermal decomposition of ammonia [31], thereby synergistically maximizing the net product yield.

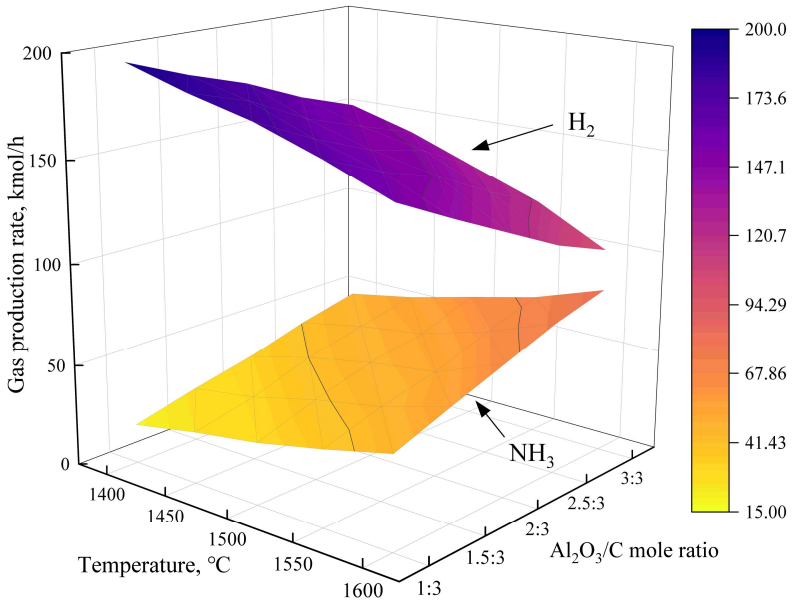


Figure 7. Effect of N-absorption reaction temperature and α-Al_2O_3/C molar ratio on NH_3 and H_2 yields.

Conversely, the total H_2 yield decreases under these conditions. This trend is dominated by the sharp reduction in H_2 generation from the decarburization reactor. As the N-absorption efficiency improves (reaching >95% carbon conversion at optimal conditions), the amount of residual carbon available for steam gasification diminishes drastically. It is noteworthy that the H_2 byproduct from the N-desorption reactor (due to ammonia decomposition) actually increases slightly due to the significantly higher total ammonia throughput, even though the specific decomposition rate is inhibited by the excess carrier. However, this minor increase is overwhelmingly outweighed by the reduction in H_2 from the decarburization step, resulting in a net decrease in total H_2 production.

3.2.2. Carbon Footprint Analysis

Figure 8 quantifies the specific CO_2 emissions per ton of ammonia. A dramatic reduction in specific emissions is observed as the operating parameters increase. Under the optimized condition (1600 °C, α-Al_2O_3/C = 3:3), the specific CO_2 emission drops to 3.2 t/t-NH_3. This value corresponds to a reduction of over 80% compared to the conventional coal-based Haber-Bosch process (~16.7 t/t-NH_3) [38]. This substantial environmental benefit validates the biomass-based CLAG process as a promising low-carbon alternative for sustainable ammonia production.

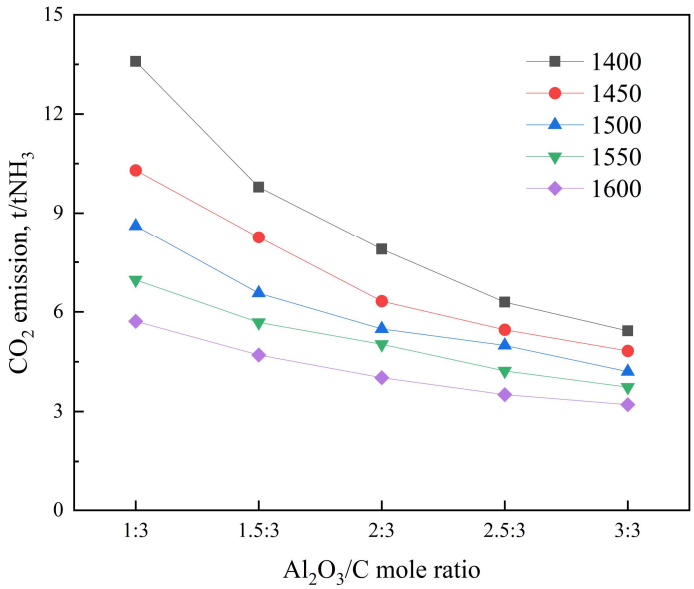


Figure 8. Effect of N-absorption reaction temperature and α-Al_2O_3/C molar ratio on CO_2 emissions.

3.3. System-Level Energy Efficiency Analysis

Evaluating the net energy efficiency is critical for determining the techno-economic feasibility of the CLAG process relative to established technologies. Unlike simplified thermodynamic models that focus solely on reaction enthalpies, this study conducts a comprehensive energy audit that rigorously accounts for the sensible heat penalties associated with high-temperature solid circulation. This holistic approach is essential for identifying realistic energy-saving opportunities and validating the system's thermal self-sufficiency.

3.3.1. Heat Duty Distribution

Figure 9 dissects the heat duty of individual components. The heat duty for the N-Absorption reactor (Figure 9a) rises with increasing reaction temperature and α-Al_2O_3/C molar ratio. This increase is inevitable as both the endothermic reaction enthalpy and the sensible heat required to raise the solid stream to the target temperature (up to 1600 °C) escalate. In contrast, the decarburization and N-desorption units (Figure 9b,c) exhibit decreasing or even negative heat duties. This is a direct consequence of the thermal inertia of the circulating solids. The solids leaving the N-absorption reactor (>1400 °C) carry immense sensible heat, which is released when they enter the lower-temperature downstream reactors (750 °C and 1075 °C). Consequently, the sensible heat carried by the solids from the high-temperature reactor is effectively utilized to satisfy the thermal requirements of these downstream units, significantly reducing their external heating demands.

Figure 9d highlights the substantial potential for energy recovery. The quantity of recoverable heat increases steadily with both the N-absorption temperature and the α-Al_2O_3/C ratio. This is because higher operating temperatures and solid circulation rates result in product gas streams (CO, H_2, N_2) with significantly higher enthalpy. Capturing this high-grade waste heat is indispensable for reducing the net external energy input required by the overall system.

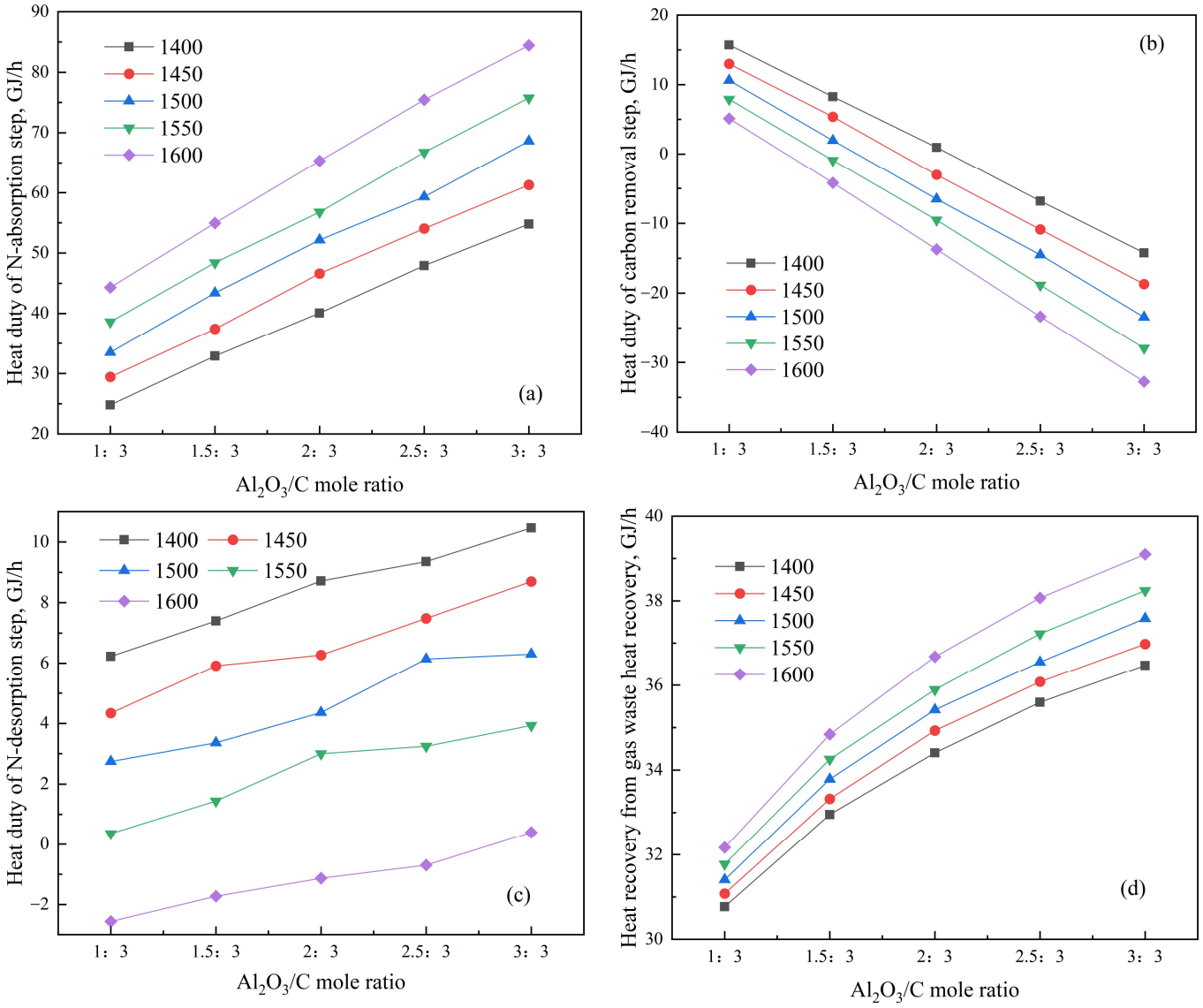


Figure 9. The effect of N-absorption reaction temperature and α-Al_2O_3/C molar ratio on the energy consumption of each component. (**a**) N-absorption step, (**b**) carbon removal step, (**c**) N-desorption step, (**d**) gas waste recovery.

3.3.2. Specific Energy Consumption Comparison

To quantitatively evaluate the system's thermodynamic performance, the total energy consumption (Q_{total}) is defined as the algebraic sum of the heat duties of all individual units, as expressed in Equation (1):

$$Q_{total} = Q_{HEATER1} + Q_{DECO} + Q_{GAS} + Q_{NAB} + Q_{REC} + Q_{NDE} + Q_{DNH} + Q_{HX7} \quad (1)$$

where $Q_{HEATER1}$, Q_{DECO}, Q_{GAS}, Q_{NAB}, Q_{REC}, Q_{NDE}, Q_{DNH} and Q_{HX7} are the energy duties associated with biomass drying, biomass pyrolysis, biomass gasification, the N-absorption reaction, decarburization, the N-desorption reaction, ammonia decomposition, and product gas waste heat recovery, respectively. Consequently, the specific energy consumption per ton of ammonia (q_N) is calculated using Equation (2):

$$q_N = Q_{total}/m_N \quad (2)$$

where m_N denotes the mass flow rate of ammonia production (t/h).

Figure 10 illustrates the variation in total energy consumption (Q_{total}). Interestingly, despite the escalating energy demand of the N-absorption unit (Figure 9a), the total system energy consumption exhibits a moderate downward trend as the reaction temperature and α-Al_2O_3/C ratio increase. This result is explained by the internal heat compensation mechanism: the increased sensible heat release in downstream reactors and the enhanced waste heat recovery (Figure 9d) effectively outweigh the higher thermal penalty of the N-absorption step.

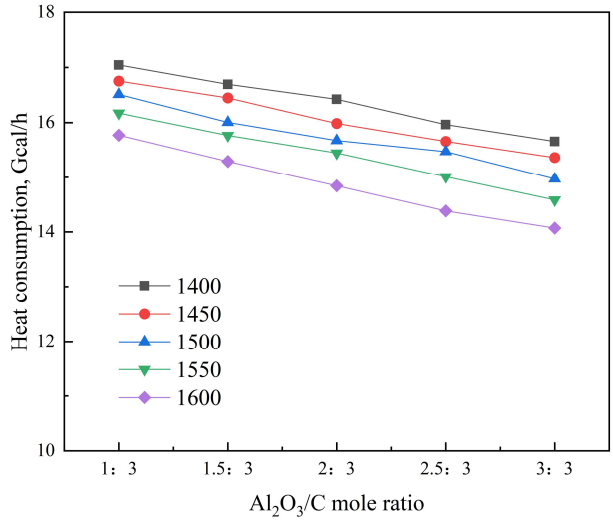


Figure 10. The effect of N-absorption reaction temperature and α-Al_2O_3/C molar ratio on total energy consumption.

Integrating these factors, Figure 11 presents the net specific energy consumption. The overall specific energy consumption decreases to a minimum of 10.12 GJ/t-NH_3 at optimal conditions. To contextualize this performance, it is compared against optimized carbon-based ammonia production routes (~27 GJ/t-NH_3) [33]. The proposed biomass-based CLAG process achieves an energy saving of over 60%. This substantial advantage is fundamentally derived from the avoidance of high-pressure compression. Unlike the conventional Haber-Bosch synthesis loop, which requires compression to 150–300 bar to overcome thermodynamic limitations and consumes vast amounts of electrical energy, the CLAG process operates at atmospheric pressure, virtually eliminating the gas compression penalty that typifies industrial ammonia synthesis.

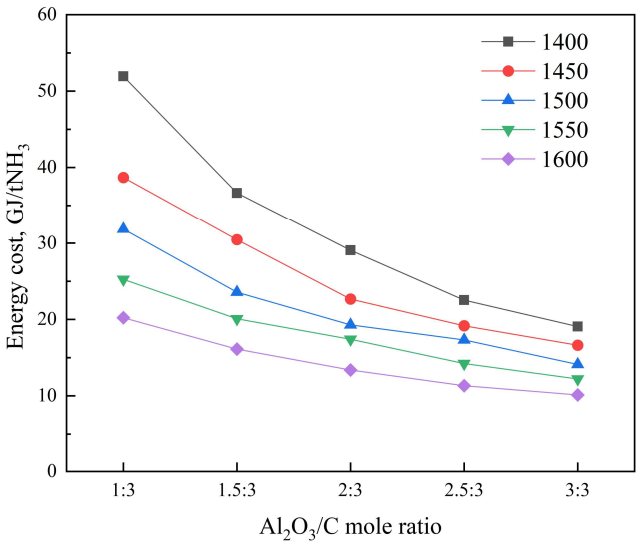


Figure 11. The effect of N-absorption reaction temperature and α-Al_2O_3/C molar ratio on energy consumption per ton of ammonia.

3.4. Energy Flow and Gas Production Analysis

Based on the comprehensive assessment of yield, carbon footprint, and specific energy consumption in the preceding sections, the operating condition of 1600 °C with an α-Al_2O_3/C ratio of 3:3 is identified as the optimal point. Before detailing the system-level energy balance, it is crucial to validate the practical feasibility of this high-temperature operation. Technically, such temperatures are standard in the metallurgical industry (e.g., Blast Furnaces) where mature refractory technologies ensure reliability. Furthermore, our 10-cycle continuous experiment (detailed data provided in the Supplementary Material, Figures S1, S2 and Table S1) confirmed that the nitrogen carrier maintains excellent structural integrity and stable reactivity (Carbon conversion ~95%) without severe sintering under these conditions. With the feasibility validated, the energy balance for this optimal scenario is visualized in the energy flow diagram (Figure 12), while the material output is detailed in the product distribution (Figure 13).

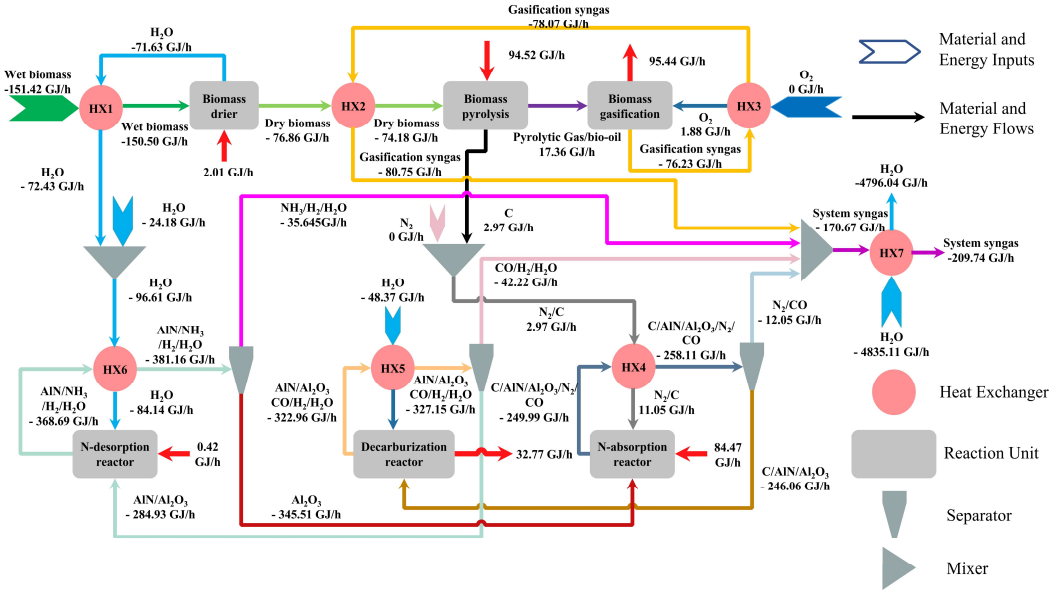


Figure 12. Diagram of energy flow in the system.

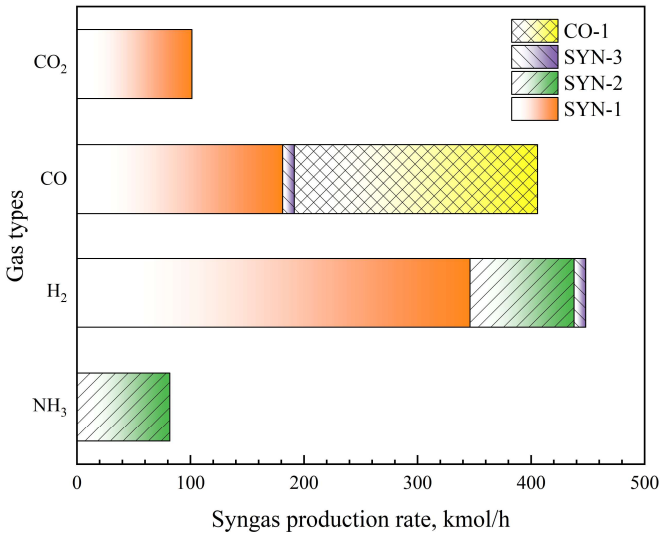


Figure 13. The total gas production of the system.

The analysis highlights the critical role of the waste heat recovery unit, which recuperates 39.08 GJ/h of high-grade heat from the product gas streams. Without this recovery, the net

energy efficiency would be severely compromised. Furthermore, Figure 13 demonstrates the system's valuable poly-generation capability. Beyond the primary ammonia product, the process co-produces substantial quantities of high-quality syngas (CO and H_2). These by-products can be utilized for power generation or downstream chemical synthesis (e.g., Fischer-Tropsch), offering economic flexibility that single-product Haber-Bosch plants lack.

4. Conclusions

This study developed a comprehensive process simulation for a biomass-based Chemical Looping Ammonia Generation (CLAG) system coupled with gasification and waste heat recovery. By incorporating experimentally derived reaction characteristics into the Aspen Plus simulation, the model provides a rigorous assessment of the system's mass and energy flows under realistic operating conditions. The primary conclusions drawn from this work are as follows:

(1) The trade-off analysis between syngas heating value and heat duty identified optimal operating conditions for the gasification unit. A temperature of 750 °C and an O2/Biomass molar ratio of 0.2 were determined as the autothermal operating point, effectively balancing the endothermic heat demand of pyrolysis with the exothermic heat release of partial oxidation, thereby maximizing energy self-sufficiency.

(2) The performance of the CLAG unit is governed by the interplay of reaction kinetics and solid circulation. Increasing the N-absorption temperature (>1400 °C) and the solid circulation ratio (α-Al_2O_3/C = 3:3) was found to significantly enhance ammonia yield. This improvement is attributed to two synergistic mechanisms: increasing the α-Al_2O_3/C ratio directly promotes the N-absorption reaction efficiency, while the residual α-Al_2O_3/C in the N-desorption reaction simultaneously facilitates ammonia generation and inhibits its thermal decomposition.

(3) Under the optimized conditions, the system achieves a remarkably low specific energy consumption of 10.12 GJ/t-NH_3 and a specific CO_2 emission of 3.2 t/t-NH_3. Compared to the conventional coal-based Haber-Bosch process, this represents an energy saving of over 60% and a carbon footprint reduction of approximately 80%. These advantages are fundamentally derived from the elimination of high-pressure gas compression and the efficient recuperation of high-grade waste heat.

(4) The analysis confirms that the proposed system is not only a single-product generator but possesses valuable poly-generation capabilities, co-producing high-quality syngas alongside ammonia. This feature enhances the system's economic flexibility. Future research should focus on a detailed techno-economic analysis (TEA) and life cycle assessment (LCA) to further validate the commercial viability and environmental impact of this technology on an industrial scale.

Supplementary Materials: The following supporting information can be downloaded at: https://www.mdpi.com/article/10.3390/pr14040588/s1, Figure S1: Conversion of N-absorption/N-desorption reactions and NH_3 yield for 10 cycles; Figure S2: Surface morphology of α-Al_2O_3 before and after cycling (a) initial; (b) after 10 cycles; Table S1: Specific surface area, total pore volume and average pore diameter of α-Al_2O_3 before and after cycling.

Author Contributions: Conceptualization, Z.L. and Q.Y.; Methodology, Z.L. and Q.Y.; Software, Z.L.; Validation, Z.L. and Q.Y.; Formal analysis, Z.L.; Investigation, Z.L., H.X., G.Y. and C.W.; Resources, Z.L., H.X., G.Y. and C.W.; Data curation, Z.L., H.X., Z.C., G.Y. and C.W.; Writing—original draft, Z.L. and L.L.; Writing—review and editing, Z.L., L.L. and Z.C.; Visualization, Z.L. and Z.C.; Supervision, Z.L. and Z.C.; Project administration, Z.L., L.L. and G.Y.; Funding acquisition, Z.L., L.L. and G.Y. All authors have read and agreed to the published version of the manuscript.

Funding: This research was funded by the China Three Gorges Corporation (NBZZ202400037), The National Key Research and Development Program of China (2017YFB0603603), and the LiaoNing Revitalization Talents Program (XLYC1802003).

Data Availability Statement: The original contributions presented in this study are included in the article/Supplementary Material. Further inquiries can be directed to the corresponding author.

Conflicts of Interest: Authors Zhongyuan Liu, Lunbo Luo, Ziwen Chen, Guangming Yu, Chen Wang were employed by the company China Three Gorges Corporation. The remaining authors declare that the research was conducted in the absence of any commercial or financial relationships that could be construed as a potential conflict of interest. The authors declare that this study received funding from the China Three Gorges Corporation. The funder was not involved in the study design, collection, analysis, interpretation of data, the writing of this article or the decision to submit it for publication.

References

1. Gezerman, A.O. A Critical Assessment of Green Ammonia Production and Ammonia Production Technologies. *Kem. Ind.* **2022**, *71*, 57–66. [CrossRef]
2. Wang, Y.; Yao, Z.; Wang, Y.; Yan, G.; Janz, B.; Wang, X.; Zhan, Y.; Wang, R.; Zheng, X.; Zhou, M.; et al. Characteristics of annual NH(3) emissions from a conventional vegetable field under various nitrogen management strategies. *J. Environ. Manag.* **2023**, *342*, 118276. [CrossRef] [PubMed]
3. Rafiqul, I.; Weber, C.; Lehmann, B.; Voss, A. Energy efficiency improvements in ammonia production—Perspectives and uncertainties. *Energy* **2005**, *30*, 2487–2504. [CrossRef]
4. Chi, W.; Yang, Q.; Chen, X.; Liu, G.; Zhao, Y.; Li, L. Performance evaluation of NH_3/CO_2 cascade refrigeration system with ejector subcooling for low-temperature cycle. *Int. J. Refrig.* **2022**, *136*, 162–171. [CrossRef]
5. Lesmana, H.; Zhang, Z.; Li, X.; Zhu, M.; Xu, W.; Zhang, D. NH_3 as a transport fuel in internal combustion engines: A technical review. *J. Energy Resour. Technol.* **2019**, *141*, 070703. [CrossRef]
6. Boretti, A.; Castelletto, S. NH_3 Prospects in Combustion Engines and Fuel Cells for Commercial Aviation by 2030. *ACS Energy Lett.* **2022**, *7*, 2557–2564. [CrossRef]
7. Zhou, M.; Wang, Y.; Chu, Y.; Tang, Y.; Tian, K.; Zheng, S.; Chen, J.; Wang, Z. Ammonia as an environmentally benign energy carrier for the fast growth of China. *Energy Procedia* **2019**, *158*, 4986–4991. [CrossRef]
8. Awad, O.I.; Zhou, B.; Harrath, K.; Kadirgama, K. Characteristics of NH_3/H_2 blend as carbon-free fuels: A review. *Int. J. Hydrogen Energy* **2022**, *48*, 38077–38100. [CrossRef]
9. Wang, Y.; Wright, L.A. A Comparative Review of Alternative Fuels for the Maritime Sector: Economic, Technology, and Policy Challenges for Clean Energy Implementation. *World* **2021**, *2*, 456–481. [CrossRef]
10. Humphreys, J.; Lan, R.; Tao, S. Development and Recent Progress on Ammonia Synthesis Catalysts for Haber–Bosch Process. *Adv. Energy Sustain. Res.* **2020**, *2*, 2000043–2000066. [CrossRef]
11. Klaas, L.; Guban, D.; Roeb, M.; Sattler, C. Recent progress towards solar energy integration into low-pressure green ammonia production technologies. *Int. J. Hydrogen Energy* **2021**, *46*, 25121–25136. [CrossRef]
12. Vojvodic, A.; Medford, A.J.; Studt, F.; Abild-Pedersen, F.; Khan, T.S.; Bligaard, T.; Nørskov, J.K. Exploring the limits: A low-pressure, low-temperature Haber–Bosch process. *Chem. Phys. Lett.* **2014**, *598*, 108–112. [CrossRef]
13. Liu, Z.; Yu, Q.; Wang, H.; Wu, J.; Tao, S. Selecting nitrogen carriers used for chemical looping ammonia generation of biomass and H_2O by thermodynamic method. *Int. J. Hydrogen Energy* **2023**, *48*, 4035–4051.
14. Xiang, P.-P.; Wang, J.-C.; Jiang, K.-J.; He, C.-M.; Jiang, W.-Y.; Guo, L.-Q.; Jiao, Y.-J.; Chen, S. Regional reallocation of zero-carbon ammonia production in China with carbon neutrality targets. *Adv. Clim. Change Res.* **2025**, *16*, 199–212. [CrossRef]
15. Chen, J.; Guan, B.; Zhuang, Z.; Zheng, C.; Zhou, J.; Su, T.; Chen, Y.; Zhu, C.; Hu, X.; Zhao, S.; et al. Recent advances of structure-performance relationship and improvement methods of catalysts for photochemical and electrochemical reduction of nitrogen to green ammonia. *Fuel* **2024**, *371*, 131928–131970. [CrossRef]
16. Wang, S.-X.; Maimaiti, H.; Xu, B.; Guo, Y.; Zhai, P.-s.; Zhang, H.-z. Fixation of Nitrogen to Ammonia with Photocatalytic on Petroleum Pitch-Based Graphene Oxide Supported Nickel/Nickel Oxide Composite Catalyst. *J. Phys. Chem. C* **2019**, *123*, 31119–31129. [CrossRef]
17. Shipman, M.A.; Symes, M.D. Recent progress towards the electrosynthesis of ammonia from sustainable resources. *Catal. Today* **2017**, *286*, 57–68. [CrossRef]
18. Ling, C.; Zhang, Y.; Li, Q.; Bai, X.; Shi, L.; Wang, J. New Mechanism for N2 Reduction: The Essential Role of Surface Hydrogenation. *J. Am. Chem. Soc.* **2019**, *141*, 18264–18270. [CrossRef]

19. Neyts, E.C.; Bogaerts, A. Understanding plasma catalysis through modelling and simulation—A review. *J. Phys. D Appl. Phys.* **2014**, *47*, 224010–224029. [CrossRef]
20. Bröer, S.; Hammer, T. Selective catalytic reduction of nitrogen oxides by combining a non-thermal plasma and a V_2O_5-WO_3/TiO_2 catalyst. *Appl. Catal. B: Environ.* **2000**, *28*, 101–111. [CrossRef]
21. Li, L.; Tang, C.; Cui, X.; Zheng, Y.; Wang, X.; Xu, H.; Zhang, S.; Shao, T.; Davey, K.; Qiao, S.Z. Efficient Nitrogen Fixation to Ammonia through Integration of Plasma Oxidation with Electrocatalytic Reduction. *Angew. Chem. Int. Ed.* **2021**, *60*, 14131–14137. [CrossRef] [PubMed]
22. Li, C.; Wang, T.; Zhao, Z.-J.; Yang, W.; Li, J.-F.; Li, A.; Yang, Z.; Ozin, G.A.; Gong, J. Promoted Fixation of Molecular Nitrogen with Surface Oxygen Vacancies on Plasmon-Enhanced TiO_2 Photoelectrodes. *Angew. Chem. Int. Ed.* **2018**, *57*, 5278–5282. [CrossRef] [PubMed]
23. Zhang, S.; Zhao, Y.; Shi, R.; Waterhouse, G.I.N.; Zhang, T. Photocatalytic ammonia synthesis: Recent progress and future. *EnergyChem* **2019**, *1*, 100013. [CrossRef]
24. Chen, J.G.; Crooks, R.M.; Seefeldt, L.C.; Bren, K.L.; Bullock, R.M.; Darensbourg, M.Y.; Holland, P.L.; Hoffman, B.; Janik, M.J.; Jones, A.K.; et al. Beyond fossil fuel-driven nitrogen transformations. *Science* **2018**, *360*, eaar6611. [CrossRef]
25. Gao, W.; Guo, J.; Wang, P.; Wang, Q.; Chang, F.; Pei, Q.; Zhang, W.; Liu, L.; Chen, P. Production of ammonia via a chemical looping process based on metal imides as nitrogen carriers. *Nat. Energy* **2018**, *3*, 1067–1075. [CrossRef]
26. Wang, B.; Yin, X.; Wang, P.; Shen, L. Chemical looping ammonia synthesis at atmospheric pressure benefiting from synergistic effect of Mn- and Fe-based nitrogen carriers. *Int. J. Hydrogen Energy* **2023**, *48*, 2705–2717. [CrossRef]
27. Gálvez, M.; Hischier, I.; Frei, A.; Steinfeld, A. Ammonia Production via a Two-Step Al_2O_3/AlN Thermochemical Cycle. 3. Influence of the Carbon Reducing Agent and Cyclability. *Ind. Eng. Chem. Res.* **2008**, *47*, 2231–2237. [CrossRef]
28. Feng, M.; Zhang, Q.; Wu, Y.; Liu, D. Using Coal Coke for N-Sorption with an Al-based Nitrogen Carrier during Chemical Looping Ammonia Generation. *Energy Fuels* **2020**, *34*, 12527–12534. [CrossRef]
29. Liu, Z.; Yu, Q.; Gao, J.; Zhao, J.; Duan, W. Effect of pyrolysis parameters on the biochar reactivity in the N-absorption reaction of chemical looping ammonia generation. *Energy* **2024**, *310*, 133321. [CrossRef]
30. Zhang, Q.; Wu, Y.; Gao, Y.; Chen, X.; Liu, D.; Fan, M. High-performance mesoporous (AlN/Al_2O_3) for enhanced NH_3 yield during chemical looping ammonia generation technology. *Int. J. Hydrogen Energy* **2020**, *45*, 9903–9913. [CrossRef]
31. Liu, Z.; Yu, Q.; Zhao, J.; Gao, J.; Duan, W. α-Al_2O_3-loaded promoted the N-desorption reaction and inhibited NH_3 decomposition in chemical looping ammonia generation: Experiments and DFT simulations. *Int. J. Hydrogen Energy* **2024**, *78*, 481–491. [CrossRef]
32. Weng, Q.; Toan, S.; Ai, R.; Sun, Z.; Sun, Z. Ammonia production from biomass via a chemical looping-based hybrid system. *J. Clean. Prod.* **2021**, *289*, 125749. [CrossRef]
33. Fang, J.; Xiong, C.; Feng, M.; Wu, Y.; Liu, D. Utilization of carbon-based energy as raw material instead of fuel with low CO_2 emissions: Energy analyses and process integration of chemical looping ammonia generation. *Appl. Energy* **2022**, *312*, 118809–118818. [CrossRef]
34. Wen, D.; Aziz, M. Design and analysis of biomass-to-ammonia-to-power as an energy storage method in a renewable multi-generation system. *Energy Convers. Manag.* **2022**, *261*, 115611. [CrossRef]
35. Kataria, G.; Sharma, A.; Joshi, J.B.; Hameed, S.; Amiri, A. A system level analysis of pyrolysis of cotton stalk biomass. *Mater. Today Proc.* **2022**, *57*, 1528–1532. [CrossRef]
36. Duan, W.; Yu, Q.; Wang, K.; Qin, Q.; Hou, L.; Yao, X.; Wu, T. ASPEN Plus simulation of coal integrated gasification combined blast furnace slag waste heat recovery system. *Energy Convers. Manag.* **2015**, *100*, 30–36. [CrossRef]
37. Liu, Z.; Yu, Q.; Xie, H.; Gao, J.; Zhao, J. Experimental and Kinetic Study of Biochar in N-Absorption Reaction of Chemical Looping Ammonia Generation. *Processes* **2024**, *12*, 2870. [CrossRef]
38. Yan, R.; Wu, M.; Fan, J.; Sun, C.; Wang, J.; He, Y.; Liu, H.; Li, P.; Zhang, J. Process integration and thermodynamic analysis of a multi-generation system including solar-assisted biomass gasification and chemical looping ammonia generation. *Energy Convers. Manag.* **2024**, *306*, 118263. [CrossRef]

Disclaimer/Publisher's Note: The statements, opinions and data contained in all publications are solely those of the individual author(s) and contributor(s) and not of MDPI and/or the editor(s). MDPI and/or the editor(s) disclaim responsibility for any injury to people or property resulting from any ideas, methods, instructions or products referred to in the content.